

Article

Induction Motor Dynamics Regimes: A Comprehensive Study of Mathematical Models and Validation

Marina Konuhova 

Institute of Solid State Physics, University of Latvia, 8 Kengaraga, LV-1063 Riga, Latvia;
marina.konuhova@cfi.lu.lv

Abstract: This study investigates the dynamic behavior of induction motors (IMs) by developing and validating four distinct mathematical models designed for transient and starting regimes. These models, expressed in α, β and d, q coordinate systems, analyze rotational frequency, electromagnetic torque, and current profiles with varying levels of complexity, including current-based, flux linkage-based, and rotor winding electromagnetic time constant approaches. Implemented in Fortran, the models address the limitations of predefined tools like MATLAB/Simulink, offering enhanced precision, flexibility, and suitability for non-standard scenarios. Validation against experimental data from a 3 kW induction motor confirms the models' accuracy, with consistent results across approaches. Notably, the flux linkage models excel in capturing intricate transient phenomena, while current-based models simplify integration with power system studies. These findings provide a robust framework for analyzing IM performance under diverse conditions such as voltage unbalance and rundown scenarios, enabling the optimization of motor operations in energy-intensive industries.

Keywords: induction motor; transients; starting mode; electromagnetic torque; modeling



Academic Editor: Roberto Zivieri

Received: 14 January 2025

Revised: 29 January 2025

Accepted: 30 January 2025

Published: 2 February 2025

Citation: Konuhova, M. Induction Motor Dynamics Regimes: A Comprehensive Study of Mathematical Models and Validation. *Appl. Sci.* **2025**, *15*, 1527.

<https://doi.org/10.3390/app15031527>

Copyright: © 2025 by the author. Licensee MDPI, Basel, Switzerland. This article is an open access article distributed under the terms and conditions of the Creative Commons Attribution (CC BY) license (<https://creativecommons.org/licenses/by/4.0/>).

1. Introduction

Induction motors with squirrel-cage rotors (IMs) are the most widely used type of electric motor [1]. They are relatively inexpensive and require minimal maintenance [2]. IMs are extensively utilized across various applications, including metalworking, woodworking, and general purpose machinery. They are also employed in press-forming, weaving, sewing, hoisting, and earth-moving equipment, as well as in fans, pumps, compressors, centrifuges, escalators, electric hand tools, household appliances, and numerous other devices [3–7]. Additionally, induction motors are commonly used in hydrogen compression systems due to their reliability, efficiency, and ease of maintenance [8–10]. It is difficult to identify any industry that does not rely on induction motors [11,12].

According to statistical data, electric motors and motor systems in industrial and infrastructure applications with pumps, fans, and compressors in buildings are responsible for 53% of the world's total electricity consumption [13] (Figure 1). This underscores the significant role of IMs as the most widely used type of electric machine in the industrial sector.

The theory of transient processes in electrical machines has been extensively developed, as demonstrated by numerous studies on this topic [14–19].

With the increase in machine capacities and their intensified usage, there has been a growing demand for higher precision in modeling complex processes in induction motors [20,21]. This has necessitated the refinement and development of motor calculation

methods. However, achieving both high precision and simplicity in the solutions simultaneously remains a persistent challenge [22].

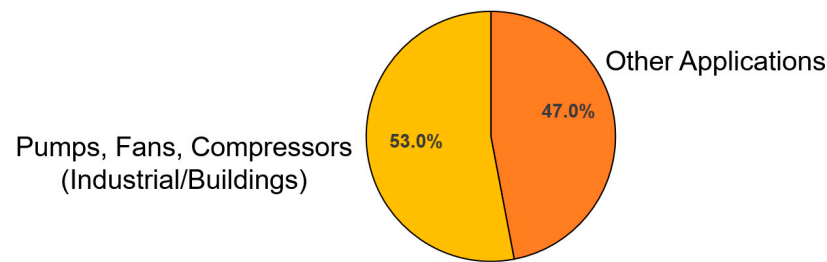


Figure 1. Global electricity consumption by electric motors.

Transient processes in induction motors (IM) are so diverse that it is impossible to study them comprehensively. As a result, research in this field is ongoing, as evidenced by a wide range of topics published in various sources. These studies primarily focus on the following aspects of IM operation: the starting regime [23,24], switching mode [25–27], operation under voltage unbalance [28–31], diagnostics [32–35], and IM parameter identification [36–42]. Transient analysis is essential for accurately predicting dynamic behaviors such as starting currents, electromagnetic torque, and speed profiles in induction motors. This understanding enables the design of appropriate protection systems, optimized switching devices, and configurations that enhance motor and network performance. By addressing challenges such as voltage unbalance and load variations, transient analysis ensures both motor efficiency and reliable operation of power systems.

Inrush currents arising in the stator and rotor windings during the starting process follow a complex oscillatory pattern [22]. The electromagnetic torque induced by these currents also exhibits oscillatory behavior and is a complex function of time [43]. Calculating the starting currents and torques of induction motors is essential for selecting appropriate protection and switching devices. Furthermore, it is crucial for assessing the permissible voltage drop in the network during motor starting, especially when the motor's capacity is comparable to that of the power supply equipment [44,45].

Transient processes do not last long. However, their effect on electric machine operation and the overall network and drive system can be significant [18]. Transient processes are more diverse and complicated than steady-state processes, which are generally transient processes particular case. Transient processes appear in electric machines when voltage, frequency, or load changes occur, such as switching machine on or off, reversing, short circuit, or parameter changes [46–48]. These processes are influenced by various factors, and their combinations can vary widely (e.g., voltage changes, frequency, equivalent parameters, or load variations). Therefore, it is essential to identify the primary influencing factors and avoid making the task overly complicated [49–52].

For induction motor transient processes research and analysis, mathematical modeling methods are widely applied [53–56]. The growing demand for precision in modeling induction motor dynamics has driven advancements in computational tools. MATLAB/Simulink, with its user-friendly interface and extensive library, is widely used for real-time modeling of dynamic regimes in induction motors [57–61]. However, Simulink has notable disadvantages, particularly in specific applications. For instance, predefined macromodules often lack transparency regarding their internal structure, which limits their adaptability for non-standard scenarios or fault conditions [62,63]. Additionally, while Simulink blocks offer ease of use through drag-and-drop functionality, their predefined functionality and options can be restrictive. Users may struggle to find blocks that suit specific needs, or they may face challenges in adjusting the behavior or appearance of existing blocks. Compatibil-

ity issues between different versions or plat-forms of Simulink can further complicate its application [62,64].

Another significant limitation of Simulink, particularly in the context of power systems and power electronics, is its computational speed. For large-scale systems, the state-space solver used by Simulink can become considerably slower than traditional solvers, such as the nodal admittance methods employed in tools like EMTP-RV and PSCAD. This drawback is especially critical in real-time applications, where low and consistent simulation time steps are essential [65].

In contrast, custom modeling approaches, such as those developed in Fortran, overcome these limitations by offering greater precision, reliability, and flexibility, particularly in scenarios requiring detailed customization [66]. Fortran's strengths enable the efficient simulation of various operating modes, including power asymmetry and transient processes, making it a robust platform for advancing the study of induction motor dynamics beyond the constraints of predefined tools. Moreover, its adaptability allows it to serve as a verification tool for validating the functionality of predefined tools like Simulink.

This study aims to address these challenges by developing mathematical models tailored for analyzing the dynamic regimes of induction motors (IMs), which are crucial in numerous industrial applications. By leveraging four distinct modeling approaches, it provides a comprehensive framework for simulating key parameters such as rotational frequency, electromagnetic torque, and current profiles under diverse operating conditions. This approach enhances the understanding of transient processes in IMs and lays the foundation for optimizing their performance, particularly in energy-intensive industries.

2. Transient Process Modeling in Induction Motor

2.1. Coordinate Conversion

To simplify the mathematical description of an induction motor (IM), coordinate system transformations and the space vector concept are often employed [67]. The goal of such transformations is to obtain equations with constant coefficients, making analysis and control easier.

This simplification is achieved using the two-axis theory, which considers not the actual magnetic flux in the air gap but its components along two mutually perpendicular axes—longitudinal and transverse (d -axis and q -axis) [68]. Coordinate transformations are widely used in technical applications to simplify complex systems by converting coordinates from one system to another. This process is known as coordinate conversion.

According to mathematical principles, the number of variables remains unchanged after a coordinate transformation. Typically, a system of equations with time-varying coefficients (e.g., in the ABC phase coordinate system) is transformed into a system with constant coefficients in the $dq0$ coordinate system.

In general, the transformation involves converting an equation system with varying coefficients in the phase coordinate system (A, B, C or 1A, 1B, 1C) into an equivalent system expressed in the $dq0$ coordinate system. This transformation simplifies the mathematical representation and facilitates the analysis and control of electrical machines [69].

An example of such a transformation is the conversion of the stator current space vector \vec{I} from the phase coordinates (1A, 1B, 1C) into the $dq0$ coordinate system (Figure 2).

If the phase currents contain a zero-sequence component, such that we define the zero-sequence component as: $(i_{1A} + i_{1B} + i_{1C})/3 = i_0$.

This zero-sequence current i_0 may vary according to any complex principle and should not be confused with the alternating zero-sequence space vector current \vec{I} .

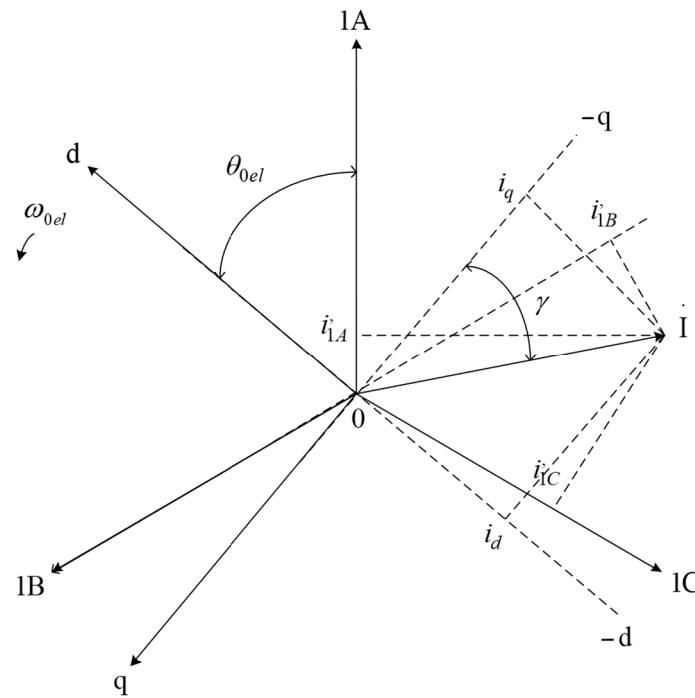


Figure 2. Current space vector.

The concept of zero-sequence current is introduced as part of the coordinate transformation methodology to provide a complete theoretical framework. However, in the context of the four models developed and analyzed in this study, zero-sequence current is not present due to the assumption of a balanced three-phase system. Under balanced conditions, the sum of the phase currents is zero, and no zero-sequence current flows. This assumption simplifies the analysis and allows the focus to remain on the primary components of transient and starting dynamics.

The coordinate axis 0 is perpendicular to the plane of the figure. In this case, the space vector \dot{I} in the ABC coordinate system can be expressed as follows: $i'_{1A} = i_{1A} - i_0$, $i'_{1B} = i_{1B} - i_0$, $i'_{1C} = i_{1C} - i_0$, such that $i'_{1A} + i'_{1B} + i'_{1C} = 0$.

Transforming the vector projections onto the phase axes provides the phase winding currents i_{1A} , i_{1B} , i_{1C} , while projections onto the rotor axes yield the currents i_d and i_q . In the general case, when the stator windings are connected in wye with a neutral wire, it is possible for $i_{1A} + i_{1B} + i_{1C} \neq 0$. In this situation, we account for the zero-sequence component as: $(i_{1A} + i_{1B} + i_{1C})/3 = i_0$, where i_0 is the stator current's zero-sequence component.

$$i_{1A} = i'_{1A} + i_0 \tag{1}$$

$$i_{1B} = i'_{1B} + i_0 \tag{2}$$

$$i_{1C} = i'_{1C} + i_0. \tag{3}$$

It should be noted that the currents marked with “prime” (e.g., i'_{1A}) no longer contain the zero-sequence component. Therefore, the currents $i'_{1A} = i_{1A} - i_0$, $i'_{1B} = i_{1B} - i_0$, $i'_{1C} = i_{1C} - i_0$ can be represented as the projections of \dot{I} onto the 1A, 1B, 1C ensuring that $i'_{1A} + i'_{1B} + i'_{1C} = 0$, as shown in Figure 2.

The relationship between the space vector components and the phase currents can be expressed as follows:

$$i'_{1A} + i'_{1B} + i'_{1C} = 0 \tag{4}$$

$$i'_{1B} = I \cos\left(\gamma + \frac{\pi}{2} - \theta_{0el} + \frac{2\pi}{3}\right) = -I \sin\left(\gamma - \theta_{0el} + \frac{2\pi}{3}\right), \tag{5}$$

$$i'_{1C} = I \cos\left(\gamma + \frac{\pi}{2} - \theta_{0el} - \frac{2\pi}{3}\right) = -I \sin\left(\gamma - \theta_{0el} - \frac{2\pi}{3}\right) \tag{6}$$

In the longitudinal axis d , and transverse axis q , the currents are given as:

$$i_d = I \cos\left(\gamma + \frac{\pi}{2}\right) = -I \sin\gamma, \tag{7}$$

$$i_q = I \cos\left(\gamma + \frac{\pi}{2}\right) = -I \sin\gamma. \tag{8}$$

Substituting Equations (4)–(6) in Equations (1)–(3) and using (7) and (8), the phase current can be expressed as:

$$i_{1A} = -I \sin\gamma \cos\theta_{0el} + I \cos\gamma \sin\theta_{0el} + i_0 = i_d \cos\theta_{0el} - i_q \sin\theta_{0el} + i_0 \tag{9}$$

$$\begin{aligned} i_{1B} &= -I \sin\gamma \cos\left(\theta_{0el} - \frac{2\pi}{3}\right) + I \cos\gamma \sin\left(\theta_{0el} - \frac{2\pi}{3}\right) + i_0 \\ &= i_d \cos\left(\theta_{0el} - \frac{2\pi}{3}\right) - i_q \sin\left(\theta_{0el} - \frac{2\pi}{3}\right) + i_0; \end{aligned} \tag{10}$$

$$\begin{aligned} i_{1C} &= -I \sin\gamma \cos\left(\theta_{0el} + \frac{2\pi}{3}\right) + I \cos\gamma \sin\left(\theta_{0el} + \frac{2\pi}{3}\right) + i_0 \\ &= i_d \cos\left(\theta_{0el} + \frac{2\pi}{3}\right) - i_q \sin\left(\theta_{0el} + \frac{2\pi}{3}\right) + i_0. \end{aligned} \tag{11}$$

Equations (9)–(11) can be written in matrix form as:

$$\begin{bmatrix} i_{1A} \\ i_{1B} \\ i_{1C} \end{bmatrix} = \begin{bmatrix} \cos\theta_{0el} & -\sin\theta_{0el} & 1 \\ \cos\left(\theta_{0el} - \frac{2\pi}{3}\right) & -\sin\left(\theta_{0el} - \frac{2\pi}{3}\right) & 1 \\ \cos\left(\theta_{0el} + \frac{2\pi}{3}\right) & -\sin\left(\theta_{0el} + \frac{2\pi}{3}\right) & 1 \end{bmatrix}. \tag{12}$$

Here, the transformation matrix is:

$$[A_1^{-1}] = \begin{bmatrix} \cos\theta_{0el} & -\sin\theta_{0el} & 1 \\ \cos\left(\theta_{0el} - \frac{2\pi}{3}\right) & -\sin\left(\theta_{0el} - \frac{2\pi}{3}\right) & 1 \\ \cos\left(\theta_{0el} + \frac{2\pi}{3}\right) & -\sin\left(\theta_{0el} + \frac{2\pi}{3}\right) & 1 \end{bmatrix} \tag{13}$$

The Park transformation matrix A_1 , is given as:

$$[A_1] = \frac{2}{3} \begin{bmatrix} \cos\theta_{0el} & -\cos\left(\theta_{0el} - \frac{2\pi}{3}\right) & \cos\left(\theta_{0el} + \frac{2\pi}{3}\right) \\ -\sin\theta_{0el} & -\sin\left(\theta_{0el} - \frac{2\pi}{3}\right) & -\sin\left(\theta_{0el} + \frac{2\pi}{3}\right) \\ \frac{1}{2} & \frac{1}{2} & \frac{1}{2} \end{bmatrix} \tag{14}$$

Using this matrix, phase currents i_{1A}, i_{1B}, i_{1C} can be transformed into $d, q, 0$ coordinates:

$$i_d = \frac{2}{3} \left[i_{1A} \cos\theta_{0el} + i_{1B} \cos\left(\theta_{0el} - \frac{2\pi}{3}\right) + i_{1C} \cos\left(\theta_{0el} + \frac{2\pi}{3}\right) \right], \tag{15}$$

$$i_q = \frac{2}{3} \left[-i_{1A} \sin\theta_{0el} - i_{1B} \sin\left(\theta_{0el} - \frac{2\pi}{3}\right) - i_{1C} \sin\left(\theta_{0el} + \frac{2\pi}{3}\right) \right] \tag{16}$$

$$i_0 = \frac{1}{3} (i_{1A} + i_{1B} + i_{1C}). \tag{17}$$

Formula (17) corresponds to i_0 expression, which was received in the beginning of chapter. Equations (15)–(17) we can obtain directly, projecting phase currents i_{1A}, i_{1B}, i_{1C} on the coordinate axes d, q . Then, received expressions should be multiplied to two out of three.

The matrices A_1^{-1} and A_1 establish the relationship between the actual stator winding currents and the transformed variables in the d , q , and 0 axes. Similarly, analogous expressions can be derived for voltages:

$$\begin{bmatrix} u_d \\ u_q \\ u_0 \end{bmatrix} = [A_1] \cdot \begin{bmatrix} u_{1A} \\ u_{1B} \\ u_{1C} \end{bmatrix} \tag{18}$$

The same transformation applies to the electromotive forces (EMFs) and flux linkages in the stator windings:

$$\begin{bmatrix} \psi_d \\ \psi_q \\ \psi_0 \end{bmatrix} = [A_1] \cdot \begin{bmatrix} \psi_{1A} \\ \psi_{1B} \\ \psi_{1C} \end{bmatrix} . \tag{19}$$

2.2. Generalized Electric Machine

The theory of electric machines traditionally examines different types of electromechanical transformations separately. This approach stems from historical developments in the field, where scientists in electromechanics established distinct theories for various machine types [70,71]. While these theories emphasize the unique features of each machine, they also highlight significant similarities in design principles and calculation methods [72].

One key similarity is the presence of a sinusoidal magnetic field in the motor air gap. To develop a generalized theory of electric machines, we consider an idealized two-pole, two-phase symmetrical electric machine. This idealized machine features mutually perpendicular windings on both the rotor and stator, as illustrated in Figure 3 [67].

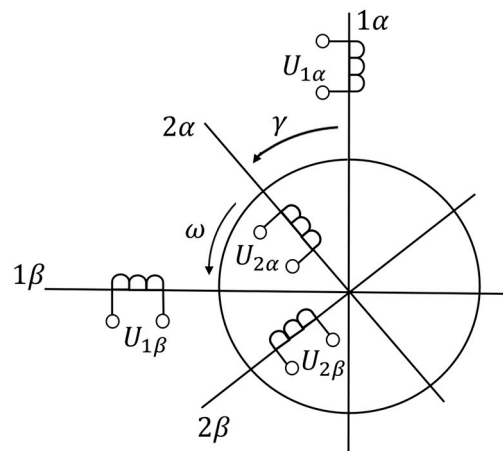


Figure 3. Generalized electric machine scheme.

A two-pole machine was selected because the processes in two-pole and multi-pole machines are analogous. In a two-pole machine, electrical radians align with geometric radians, simplifying the comparison of the rotor position relative to the stator phases, especially during transient processes. In a two-phase machine, spatially displacing the windings by $\pi/2$ generates a circular magnetic field. This configuration combined with a uniform air gap eliminates mutual inductive coupling between windings and simplifies the machine equations. For this reason, three-phase machines are frequently converted into two-phase machines for analytical purposes [73,74].

The generalized electric machine assumes a uniform air gap, with no slots on the stator or rotor. They are modeled as current layers with a sinusoidal magnetomotive force distribution. Feeding the windings with alternating current produces a sinusoidal magnetic field in the air gap, given the uniform magnetic circuit and the absence of saturation. This

generalized model represents a pair of intermoving windings and serves as a mathematical framework to analyze the processes in various electric machines. By reducing real machines to this model, operating and transient processes can be studied more effectively [75].

The mathematical model of the generalized electric machine consists of a system of differential equations. These include equilibrium equations for the winding voltages and a torque balance equation describing the machine’s motion. For simplicity, rotor winding parameters are reduced to the stator side, with the reduction factors omitted for clarity.

In the $1\alpha, 1\beta$ and $2\alpha, 2\beta$ coordinate systems, the following equations govern the system [22]:

$$U_{1\alpha} = R_1 i_{1\alpha} + \frac{d}{dt} \psi_{1\alpha}, \tag{20}$$

$$U_{1\beta} = R_1 i_{1\beta} + \frac{d}{dt} \psi_{1\beta}, \tag{21}$$

$$U_{2\alpha} = R_2 i_{2\alpha} + \frac{d}{dt} \psi_{2\alpha}, \tag{22}$$

$$U_{2\beta} = R_2 i_{2\beta} + \frac{d}{dt} \psi_{2\beta}. \tag{23}$$

Here:

$U_{1\alpha}, U_{1\beta}, U_{2\alpha}, U_{2\beta}$ are the applied voltages in the stator and rotor windings;

$i_{1\alpha}, i_{1\beta}, i_{2\alpha}, i_{2\beta}$ represent the winding currents;

R_1, R_2 are the stator and rotor winding resistances, respectively.

The rotor’s motion is described by the equation:

$$T_e = T_l + J \frac{d\Omega}{dt}, \tag{24}$$

where

T_e is the electromagnetic torque generated by the machine;

T_l is the applied load torque;

$J \frac{d\Omega}{dt}$ is the dynamic torque;

J represents the combined inertia of the rotor and any connected equipment (reduced to the rotor shaft);

Ω is the angular velocity. For a generalized electric machine, when $2p = 2, \Omega = \omega$.

These equations comprehensively describe both dynamic and static behaviors of a generalized electric machine. Given the stator voltage \dot{U}_1 and rotor voltage \dot{U}_2 :

$$\dot{U}_1 = U_{1m} \cdot e^{j(\omega_1 t + \alpha_0)} = U_{1m} [\cos(\omega_1 t + \alpha_0) + j \sin(\omega_1 t + \alpha_0)] \tag{25}$$

$$\dot{U}_2 = U_{2m} \cdot e^{j(\omega_2 t + \alpha_2)} = U_{2m} [\cos(\omega_2 t + \alpha_2) + j \sin(\omega_2 t + \alpha_2)] \tag{26}$$

where

ω_1 —is the angular frequency of the supply network;

ω_2 —is the angular frequency of \dot{U}_2 relative to the rotor axes;

α_0 —is the initial phase angle of \dot{U}_1 relative to the 1α axis at $t = 0$;

α_2 —is the initial phase angle of \dot{U}_2 relative to the 2α axis at $t = 0$.

It is evident that the system of differential Equations (20)–(24) generally does not have a straightforward solution, as the coefficients in the flux linkage equations are time-dependent. The coordinate system $1\alpha, 1\beta$ is fixed, while the $2\alpha, 2\beta$ coordinate system rotates at the angular speed ω of the rotor.

2.3. Generalized Machine in a Common Coordinate System Rotating at Arbitrary Speed

The mutual immobility of the stator and rotor magnetic fields can be achieved under the following conditions:

- The rotor’s rotating windings are conceptually treated as stationary (braked); or
- The stator’s stationary windings are assumed to rotate at the same speed as the rotor.

Additionally, the frequencies of the currents must be adjusted to align with these conditions. To preserve power invariance and operate with actual amplitudes of voltages and currents, an electromotive rotational force is introduced into the voltage and current balance equations.

To generalize, we transform the equations of an electric machine into the x, y coordinate system. This system is common to both the stator and rotor and rotates at an arbitrary angular speed (see Figure 4).

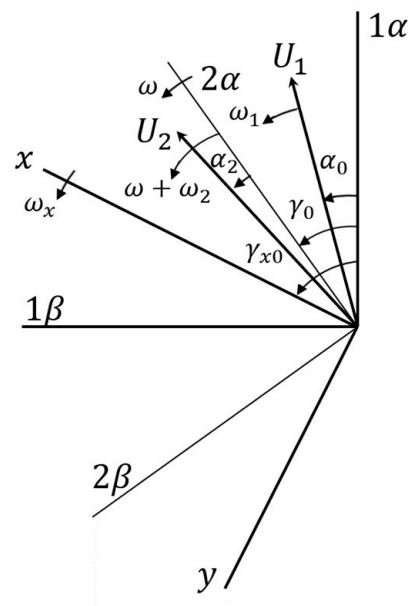


Figure 4. Coordinate system and voltages space vectors.

The stator voltage balance equation, expressed in terms of space vectors $\dot{U}_1, \dot{\psi}_1, \dot{I}_1$, is given by:

$$\dot{U}_1 = R_1 \dot{I}_1 + \frac{d\dot{\psi}_1}{dt} \tag{27}$$

To account for the rotational difference between the stationary $1\alpha, 1\beta$ coordinate system and the rotating x, y coordinate system, the equation is multiplied by $e^{-j(\omega_x t + \gamma_{x0})}$.

$$\dot{\psi}_1(x, y) = \dot{\psi}_1 e^{-j(\omega_x t + \gamma_{x0})} = \psi_{1m} e^{j((\omega_1 - \omega_x)t + \alpha_0 - \gamma_{x0} - \phi)}; \tag{28}$$

$$\begin{aligned} \dot{U}_1(x, y) &= \dot{U}_1 \cdot e^{-j(\omega_x t + \gamma_{x0})} = U_{1m} \cdot e^{j(\omega_1 t + \alpha_0)} \cdot e^{-j(\omega_x t + \gamma_{x0})} = \\ &= U_{1m} \cdot e^{j((\omega_1 - \omega_x)t + \alpha_0 - \gamma_{x0})}; \end{aligned} \tag{29}$$

$$\dot{I}_1(x, y) = \dot{I}_1 e^{-j(\omega_x t + \gamma_{x0})} = I_{1m} \cdot e^{j((\omega_1 - \omega_x)t + \alpha_0 - \gamma_{x0} - \phi)}. \tag{30}$$

where ϕ represents the displacement angle between the vectors $\dot{\psi}_1$ and \dot{I}_1 relative to \dot{U}_1 at $t = 0$.

The time derivative of the flux linkage is expressed as:

$$\frac{d\dot{\psi}_1(x, y)}{dt} = \frac{d}{dt} \left\{ \dot{\psi}_1 \cdot e^{-j(\omega_x t + \gamma_{x0})} \right\} = \left(\frac{d\dot{\psi}_1}{dt} \right) \cdot e^{-j(\omega_x t + \gamma_{x0})} - j\omega_x \dot{\psi}_1 e^{-j(\omega_x t + \gamma_{x0})}. \tag{31}$$

Substituting, the stator voltage balance in the x, y coordinate system becomes:

$$\dot{U}_1(x, y) = R_1 \dot{I}_1(x, y) + \frac{d\dot{\psi}_1(x, y)}{dt} + j\omega_x \dot{\psi}_1(x, y). \tag{32}$$

Separating real and imaginary parts, the voltage balance equations in the x, y coordinate axes are:

$$\left. \begin{aligned} U_{1x} &= \frac{d\psi_{1x}}{dt} - \omega_x \psi_{1y} + R_{1y} + R_1 i_{1x} \\ U_{1y} &= \frac{d\psi_{1y}}{dt} - \omega_x \psi_{1x} + R_{1y} + R_1 i_{1y} \end{aligned} \right\} \tag{33}$$

For the rotor windings, the voltage balance equation is:

$$\dot{U}_2 = \frac{d\dot{\psi}_2}{dt} + R_2 \dot{I}_2. \tag{34}$$

Multiplying by $e^{-j((\omega - \omega_x)t + \gamma_0 - \gamma_{x0})}$ to account for the rotational difference between the $2\alpha, 2\beta$ and x, y systems, and applying similar transformations, we obtain:

$$\dot{U}_2(x, y) = \frac{d\dot{\psi}_2(x, y)}{dt} + j(\omega - \omega_2) \dot{\psi}_2(x, y) + R_2 \dot{I}_2(x, y). \tag{35}$$

Breaking this into components yields:

$$\left. \begin{aligned} U_{2x} &= \frac{d\psi_{2x}}{dt} - (\omega - \omega_x) \psi_{2y} + R_2 i_{2x} \\ U_{2y} &= \frac{d\psi_{2y}}{dt} - (\omega - \omega_x) \psi_{2x} + R_2 i_{2y} \end{aligned} \right\}. \tag{36}$$

By appropriately selecting the angular frequencies $\omega_1, \omega_2, \omega, \omega_x$, the induction machine can be analyzed in any coordinate system.

A key feature of this model is the inclusion of rotational electromotive forces: $\omega_x \psi_{1y}, \omega_x \psi_{1x}, (\omega - \omega_x) \psi_{2y}, (\omega - \omega_x) \psi_{2x}$. In the x, y coordinate system (common to both stator and rotor), the machine windings behave as semi-fixed, resulting in flux linkages without alternating coefficients:

$$\psi_{1x} = L_{1x} i_{1x} + L_m i_{2x} \psi_{1y} = L_{1y} i_{1y} + L_m i_{2y} \psi_{2x} = L_m i_{1x} + L_{2x} i_{2x} \psi_{1y} = L_m i_{1y} + L_{2y} i_{2y}$$

3. Models of Induction Motors

3.1. Induction Motor Model in the $\alpha\beta$ Coordinate System

For α, β ($\omega_x = 0$) fixed coordinate system with axes linked to the stator, Equations (33) and (36) solving relative to flux linkages derivatives take the following form:

$$\left. \begin{aligned} \frac{d\psi_{1\alpha}}{dt} &= U_m \cos(\tau) - R_1 i_{1\alpha} \\ \frac{d\psi_{1\beta}}{dt} &= U_m \sin(\tau) - R_1 i_{1\beta} \\ \frac{d\psi_{2\alpha}}{dt} &= -R_2 i_{2\alpha} + \omega \psi_{2\beta} \\ \frac{d\psi_{2\beta}}{dt} &= -R_2 i_{2\beta} + \omega \psi_{2\alpha} \end{aligned} \right\} \tag{37}$$

The rotor speed variation is described by the following equation:

$$\frac{d\omega}{dt} = (T_e - T_l) / T_M \tag{38}$$

where T_e is the electromagnetic torque, T_l is the load torque, and T_M represents the motor's moment of inertia.

The current components are determined using the flux linkage expressions:

$$\left. \begin{aligned} i_{1\alpha} &= \frac{(X_2\psi_{1\alpha} - X_{ad}\psi_{2\alpha})}{\Delta} \\ i_{1\beta} &= \frac{(X_2\psi_{1\beta} - X_{ad}\psi_{2\beta})}{\Delta} \\ i_{2\alpha} &= \frac{(X_1\psi_{2\alpha} - X_{ad}\psi_{1\alpha})}{\Delta} \\ i_{2\beta} &= \frac{(X_1\psi_{2\beta} - X_{ad}\psi_{1\beta})}{\Delta} \end{aligned} \right\} \quad (39)$$

where

$$\Delta = X_1X_2 - X_{ad}X_{ad}$$

The electromagnetic torque is given by:

$$T_e = X_{ad}(i_{1\alpha}i_{2\beta} - i_{1\beta}i_{2\alpha}) \quad (40)$$

and the load torque is the following:

$$T_l = SM\omega_2^2 + SMC \quad (41)$$

where

$\psi_{1\beta}, \psi_{1\alpha}, \psi_{2\beta}, \psi_{2\alpha}$ are the stator and rotor flux linkage components in the $\alpha\beta$ coordinate system,

$i_{1x}, i_{1y}, i_{2x}, i_{2y}$ are the stator and rotor current components in the $\alpha\beta$ coordinate system,

ω is the rotor angular speed,

$U_m\cos(\tau), -U_m\sin(\tau)$ are the stator applied voltage,

$R_1, R_2, X_1, X_2, X_{ad}$ are the induction motor parameters in per-unit values,

T_e, T_l are the electromagnetic and load torques, respectively,

SM, SMC are the motor's variable and constant torques coefficients.

The developed induction motor model in the $\alpha\beta$ coordinate system provides a framework for simulating various dynamic operating modes, including direct starting and direct starting with current displacement in the slots. This model (*model I*) enables direct comparisons between the single-phase simulation results and the experimental data, without additional transformations.

3.2. The Model of the Induction Motor in the d,q Coordinate System

Using Equations (33) and (36), we can express the induction motor model in matrix form as follows:

$$\begin{bmatrix} u_{1d} \\ u_{1q} \\ 0 \\ 0 \end{bmatrix} = \begin{bmatrix} R_a & 0 & 0 & 0 \\ 0 & R_a & 0 & 0 \\ 0 & 0 & R_2 & 0 \\ 0 & 0 & 0 & R_2 \end{bmatrix} \cdot \begin{bmatrix} i_{1d} \\ i_{1q} \\ i_{2d} \\ i_{2q} \end{bmatrix} + \begin{bmatrix} -\omega_{0el}\psi_{1q} \\ \omega_{0el}\psi_{1d} \\ -(\omega_x - \omega)\psi_{2q} \\ (\omega_x - \omega)\psi_{2d} \end{bmatrix} + \frac{d}{dt} \begin{bmatrix} \psi_{1d} \\ \psi_{1q} \\ \psi_{2d} \\ \psi_{2q} \end{bmatrix}, \quad (42)$$

$$\frac{d\omega}{dt} = [X_{ad}(i_{2d}i_{1q} - i_{2q}i_{1d}) - T_l], \quad (43)$$

where flux linkages derivatives can be expressed as:

$$\frac{d}{dt} \begin{pmatrix} i_{1d} \\ i_{1q} \\ i_{2d} \\ i_{2q} \end{pmatrix} = \begin{pmatrix} -C_1 R_1 & +C_1 f_1 & +C_1 X_{ad} & +C_1 X_{ad} \omega \\ -C_1 f_1 & -C_1 R_1 & -C_1 X_{ad} \omega & +C_2 X_{ad} \\ C_3 R_1 & -X_1 f_2 & -C_2 X_1 & -f_3 \\ X_1 f_2 & +C_3 R_1 & +f_3 & -C_2 X_1 \end{pmatrix} * \begin{pmatrix} i_{1d} \\ i_{1q} \\ i_{2d} \\ i_{2q} \end{pmatrix} + \begin{pmatrix} C_1 & 0 & 0 & 0 \\ 0 & C_1 & 0 & 0 \\ 0 & 0 & C_1 & 0 \\ 0 & 0 & 0 & C_1 \end{pmatrix} * \begin{pmatrix} U_{1d} \\ U_{1q} \\ U_{2d} \\ U_{2q} \end{pmatrix}, \tag{44}$$

where u_{1d}, u_{1q} stator applied voltages;

$i_{1d}, i_{1q}, i_{2d}, i_{2q}$ stator and rotor currents components in the d, q coordinate system;

$\psi_{1d}, \psi_{1q}, \psi_{2d}, \psi_{2q}$ stator and rotor flux linkages component in d, q coordinate system;

The constants are defined as:

$$C_1 = \frac{1}{X_d'} = \frac{1}{X_1 - \frac{X_{ad}^2}{X_2}}, C_2 = \frac{R_2}{X_2} \cdot C_1, C_3 = \frac{X_{ad}}{X_2} \cdot C_1, f_1 = \left(X_1 - \frac{X_{ad}^2}{X_2} \right) \omega_x + \frac{X_{ad}^2}{X_2}$$

$$f_2 = \omega \cdot C_3, f_3 = (C_1 X_1 (\omega - \omega_x)).$$

Thus, this model provides a framework for solving the induction motor (IM) equations in terms of currents. The IM model in the d, q coordinate system (referred to as model II) is expressed using current variables, enabling its integration into studies analyzing the motor’s impact on power supply systems.

3.3. The Model of the Induction Motor in the d, q Coordinate System in Flux Linkages

If Equations (33) and (36) are rewritten in terms of flux linkage derivatives, the system of equations takes the following form:

$$\left. \begin{aligned} \frac{d\psi_{1d}}{dt} &= U_{1d} - R_1 i_{1d} + \omega \psi_{1q} \\ \frac{d\psi_{1q}}{dt} &= U_{1q} - R_1 i_{1q} - \omega \psi_{1d} \\ \frac{d\psi_{2d}}{dt} &= -R_2 i_{2d} + (\omega_x - \omega) \psi_{2d} \\ \frac{d\psi_{2q}}{dt} &= -R_2 i_{2q} - (\omega_x - \omega) \psi_{2d} \end{aligned} \right\}, \tag{45}$$

The torque balance equation is given by:

$$T_M \frac{d\omega}{dt} = [T_e - T_l], \tag{46}$$

where the electromagnetic torque is expressed as:

$$T_e = X_{ad} (i_{2d} i_{1q} - i_{2q} i_{1d}).$$

The stator and rotor currents can be expressed in terms of flux linkages as:

$$\left. \begin{aligned} i_{1d} &= (X_2 \cdot \psi_{1d} - X_{ad} \cdot \psi_{2d}) / \Delta \\ i_{1q} &= (X_2 \cdot \psi_{1q} - X_{ad} \cdot \psi_{2q}) / \Delta \\ i_{2d} &= (X_1 \cdot \psi_{2d} - X_{ad} \cdot \psi_{1d}) / \Delta \\ i_{2q} &= (X_1 \cdot \psi_{2q} - X_{ad} \cdot \psi_{1q}) / \Delta \end{aligned} \right\}, \tag{47}$$

where $\Delta = X_1 X_2 - X_{ad} X_{ad}$.

Equations (45)–(47) represent the mathematical model of the induction motor (IM) in terms of flux linkages. This IM model, expressed in the d,q coordinate system (referred to as model III) enables the analysis of motor operation in autonomous regimes, including scenarios where the motor operates independently or is connected to a power supply network with an infinitely large capacity.

3.4. Induction Motor Model in Flux Linkages with Rotor Windings Electromagnetic Time Constant in d,q Coordinate System

If Equations (33) and (36) are reformulated to include flux linkages with rotor windings' electromagnetic time constant derivatives, the system of equations is as follows:

$$\left. \begin{aligned} U_d &= \frac{d\psi_{1d}}{dt} - \omega\psi_{1q} + R_1 i_d \\ U_q &= \frac{d\psi_{1q}}{dt} + \omega\psi_{1d} + R_1 i_q \\ 0 &= -\frac{d\psi_{2d}}{dt} - \frac{\psi_{1d}}{T_R} - \frac{X_{ad}}{T_R} i_d + \psi_{2q}(\omega_{0el} - \omega) \\ 0 &= -\frac{d\psi_{2q}}{dt} - \frac{\psi_{1q}}{T_R} + \frac{X_{ad}}{T_R} i_q - \psi_{2d}(\omega_{0el} - \omega) \end{aligned} \right\}, \tag{48}$$

where T_e the electromagnetic torque, is calculated as:

$$T_e = X_{ad}(i_{2d}i_{1q} - i_{2q}i_{1d}).$$

The currents can be expressed in terms of flux linkages:

$$\left. \begin{aligned} i_{1d} &= (X_2 \cdot \psi_{1d} - X_{ad} \cdot \psi_{2d}) / \Delta \\ i_{1q} &= (X_2 \cdot \psi_{1q} - X_{ad} \cdot \psi_{2q}) / \Delta \\ i_{2d} &= (X_1 \cdot \psi_{2d} - X_{ad} \cdot \psi_{1d}) / \Delta \\ i_{2q} &= (X_1 \cdot \psi_{2q} - X_{ad} \cdot \psi_{1q}) / \Delta \end{aligned} \right\}, \tag{49}$$

where $\Delta = X_1 X_2 - X_{ad} X_{ad}$.

Model IV incorporates the rotor winding electromagnetic time constant, a critical parameter governing the evolution of flux linkages and currents within the rotor circuit during transient events. This time constant directly influences the motor's response to rapid changes in voltage, load, or other external conditions. For example, during starting or voltage dips, it determines the decay rate of transient components and the stabilization of steady-state performance. By accounting for this parameter, Model IV enables accurate analysis of motor parameter variations during rundown regimes and transient phenomena, such as torque oscillations and current peaks. This detailed modeling is essential for motor protection and optimizing system performance, offering insights beyond those achievable with simpler models.

4. Induction Motor Starting Mode Modeling

To calculate the starting mode of an induction motor (IM), including current, rotational frequency, and electromagnetic torque under no-load conditions, the following IM models were used: model I—expressed in the α,β coordinate system, model II—in the d,q coordinate systems using currents, model III—in the d,q coordinate systems using flux linkages and model IV—in the d,q coordinate system using flux linkages with the rotor winding electromagnetic time constant.

For starting mode modeling, the parameters of a 3 kW induction motor with the following per unit (pu) values were used [76]: $X_1 = 0.057$ pu, $X_{ad} = 3.4$ pu, $X_2 = 0.1$ pu, $R_1 = 0.072$ pu, $R_2 = 0.0487$ pu, $T_M = 32.986$.

Figure 5 illustrates the rotational frequency characteristics of a 3 kW induction motor during starting mode under no-load conditions. The graph shows the rotor’s acceleration profile, demonstrating how the rotational frequency stabilizes as the motor reaches a steady-state operation.

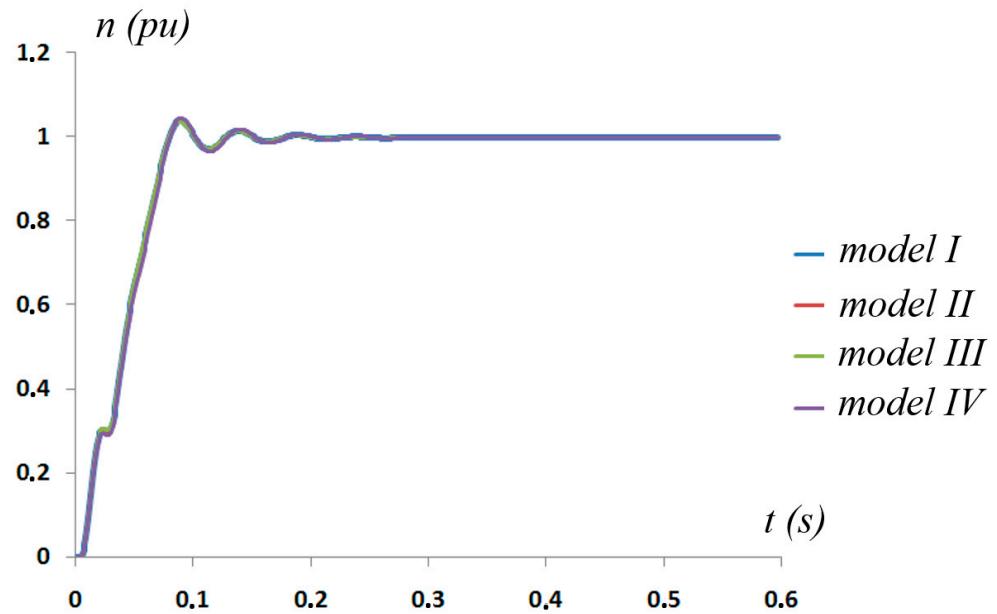


Figure 5. Rotational frequency during the starting mode of a 3 kW induction motor under no-load conditions.

Figure 6 illustrates the current drawn by the induction motor during direct starting under no-load conditions. The graph highlights the initial high inrush current, which gradually decreases as the motor transitions to steady-state operation.

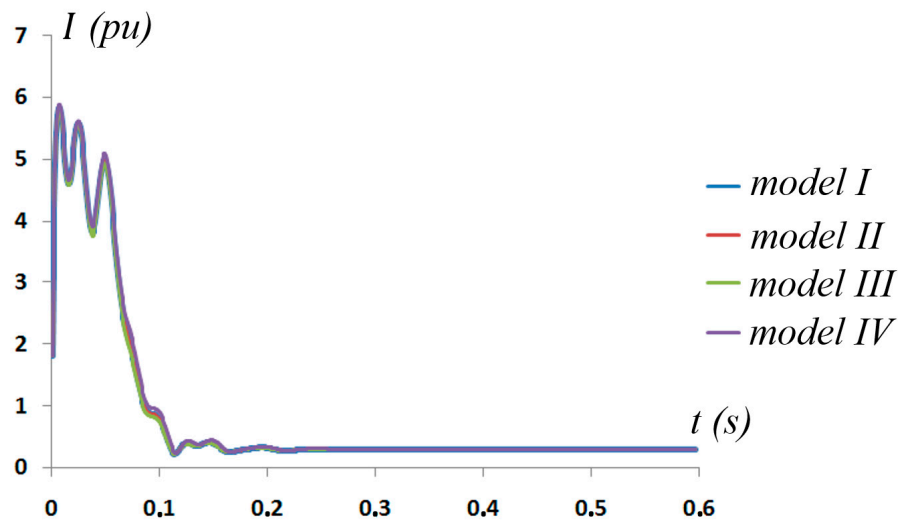


Figure 6. Current drawn during direct starting of a 3 kW induction motor under no-load conditions.

Figure 7 shows the variation in electromagnetic torque during the starting phase of the induction motor. The torque curve emphasizes the transient behavior before stabilizing at its no-load steady-state value.

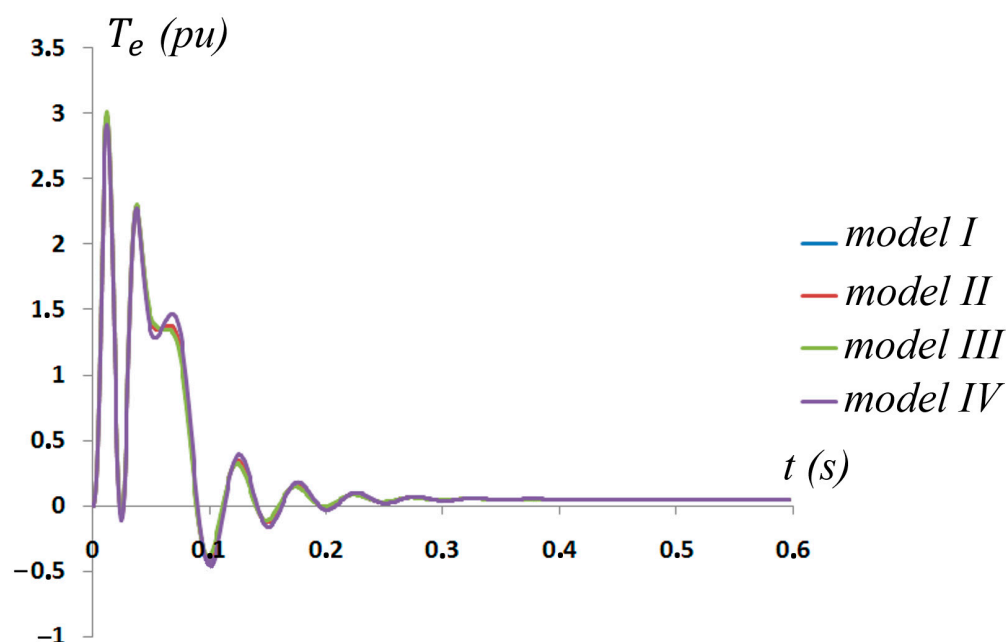


Figure 7. Electromagnetic torque variation during the starting phase of a 3 kW induction motor under no-load conditions.

Mathematical modeling of the IM starting mode, based on the models presented earlier in this paper, reveals that regardless of the coordinate system chosen (α, β or d, q) or the mathematical basis (currents, flux linkages, or flux linkages with rotor windings' electromagnetic time constant), the modeling results are consistent and accurately represent real-world behavior. The results of the starting mode mathematical modeling using Model I were compared with experimental data from a test setup described in [22], which included measurements of current, rotational speed, and torque using specialized equipment. These comparisons demonstrated close alignment between modeled and experimental results, validating the model's accuracy and reliability for analyzing IM starting dynamics.

The data tables in Appendix A show that the values of current, rotational frequency, and electromagnetic torque are in close agreement across the four models, particularly at later time instances. However, minor discrepancies are observed during the initial period, which can be attributed to transient effects. Despite these variations, the models converge to similar steady-state behavior, indicating that any of these models can be effectively used to simulate the dynamic regimes of induction motors, provided that the transient period is appropriately considered.

In addition to the no-load starting characteristics presented in Figures 5–7, the four presented IM models can also simulate starting regimes for induction motors of various capacities, with different load characteristics and torque profiles. This flexibility ensures broad applicability of these models for analyzing and optimizing motor performance under diverse operational conditions.

A comparative summary of the four mathematical models is presented in Table 1. The table outlines the coordinate systems, key parameters simulated, and the strengths and limitations of each model. This summary provides additional context for understanding the unique features and applications of the models, helping to identify their suitability for different dynamic regimes of induction motor operation.

Table 1. Comparative summary of the four mathematical models for induction motor analysis.

Model	Coordinate System Type	Key Parameters Simulated	Key Features	Applications
I	α, β	Rotational frequency, current, torque	Simple implementation, direct experimental comparison	Suitable for basic dynamic studies and starting scenarios under no-load
II	d, q (Current)	Rotational frequency, current, torque	Enables integration of the motor's mathematical model to evaluate its impact on the power supply system	Suitable for analyzing voltage unbalance, grid interaction, and power system effects during starting
III	d, q (Flux linkage)	Rotational frequency, current, torque, flux linkages	Supports the analysis of autonomous operation regimes for motors fed by a power supply system with infinite capacity	Effective for stand-alone motor analysis and advanced control strategy development
IV	d, q (Flux linkages with rotor constant)	Parameter variations during rundown	Analyzes motor parameter changes during rundown, emphasizing the rotor windings' electromagnetic time constant.	Useful for studying transient torque oscillations and motor response during rundown scenarios

The choice of modeling approach affects both the computational complexity and the focus of the analysis. Current-based models are simpler and often preferred for analyzing motor impacts on power systems, as they directly relate to electrical network interactions. On the other hand, flux linkage-based models offer deeper insights into the internal electromagnetic behavior of the motor, making them more suitable for advanced control strategies and detailed transient analyses. Both approaches provide consistent results under equivalent conditions, but their selection depends on the specific objectives of the analysis, such as whether the focus is on external power supply interactions or intrinsic motor dynamics.

Before concluding, it is worth noting that the results of this study may be relevant for the development of other types of electric machines, as well as for applications involving advanced signal processing techniques, such as adaptive step-size forward-backward pursuit and acoustic emission-based health state assessment of high-speed train bearings [77].

5. Conclusions

This study developed and evaluated four distinct mathematical models for analyzing the dynamic behavior of induction motors during starting and transient processes. The models, based on the α, β and d, q coordinate systems with variations in current and flux linkage representation, produced consistent results regardless of the chosen modeling approach. This consistency was validated through numerical simulations and comparison with experimental data, confirming the accuracy and reliability of the models.

The implementation of the models in Fortran provided enhanced computational flexibility, allowing precise simulation of key parameters, such as rotational frequency, electromagnetic torque, and current profiles. Additionally, the models facilitate the analysis of motor operation under various conditions, including voltage unbalance, starting modes, and rundown scenarios.

A significant finding is that any of the four models can be effectively used to study induction motor dynamics without compromising accuracy. For instance, the rotational frequency results for the 3 kW induction motor during starting mode stabilized at approximately 0.998 pu across all models, demonstrating their consistency. The maximum inrush current during startup reached around 5.6 pu, gradually decreasing to steady-state values close to 0.292 pu. The electromagnetic torque exhibited transient peaks of about 2.46 pu

before stabilizing near 0.05 pu. These values closely align with experimental results, further validating the accuracy and reliability of the proposed mathematical models for induction motor dynamics.

The choice of the appropriate model depends on the specific application. Model I is the simplest and is well-suited for basic analysis and direct experimental comparisons under no-load conditions. Model II is ideal for grid interaction studies, including voltage unbalance and power system analysis. For more detailed transient analyses and advanced control strategy development, Models III and IV are recommended, with Model IV being particularly effective for scenarios involving the rotor winding electromagnetic time constant, such as rundown and transient torque oscillations.

Future work will focus on utilizing the developed models to investigate induction motor operating modes under various conditions, including unbalanced voltages, asymmetry, rundown mode, switching mode, and other dynamic scenarios. This continued investigation aims to enhance the understanding of specific transient behaviors and refine the models for studying a broader range of dynamic regimes, providing valuable insights into the operational characteristics of induction motors.

Funding: M.K. thanks the Institute of Solid State Physics, University of Latvia (ISSP UL), which is as the Center of Excellence is supported through the European Union Horizon 2020 Framework Pro-gramme H2020-WIDESPREAD-01-2016-2017-TeamingPhase2 under grant agreement No. 739508, project CAMART2.

Institutional Review Board Statement: Not applicable.

Informed Consent Statement: Not applicable.

Data Availability Statement: The data and Fortran code supporting the findings of this study are available from the corresponding author upon reasonable request.

Acknowledgments: M.K. thanks Anatoli Popov for fruitful discussion.

Conflicts of Interest: The author declares no conflicts of interest.

Appendix A

Tables A1–A3 present the calculated values for rotational frequency, current, and electromagnetic torque during the starting mode of a 3 kW induction motor. The results were obtained using four mathematical models:

Model I: Induction motor (IM) model in the α, β coordinate axes.

Model II: IM model in the d, q coordinate axes using currents,

Model III: IM model in the d, q coordinate axes using flux linkages,

Model IV: IM model in the d, q coordinate axes using flux linkages with the rotor time constant.

The tables highlight the motor's transient and steady-state performance, with particular attention to how each model handles initial conditions and stabilization.

Table A1. IM rotation frequency n (pu).

t (s)	Model I	Model II	Model III	Model IV
0.01	0.069	0.069	0.07	0.067
0.05	0.643	0.643	0.65	0.625
0.1	1.005	1.005	1.003	1.011
0.15	1.001	1.001	1.00	1.004
0.2	0.999	0.999	0.998	1.00

Table A1. *Cont.*

t (s)	Model I	Model II	Model III	Model IV
0.25	0.998	0.998	0.998	0.998
0.3	0.998	0.998	0.998	0.998
0.35	0.998	0.998	0.998	0.998
0.4	0.998	0.998	0.998	0.998
0.45	0.998	0.998	0.998	0.998
0.5	0.998	0.998	0.998	0.998
0.55	0.998	0.998	0.998	0.998
0.6	0.998	0.998	0.998	0.998

Table A2. IM current I (pu).

t (s)	Model I	Model II	Model III	Model IV
0.01	5.585	5.585	5.557	5.647
0.05	4.977	4.977	4.925	5.087
0.1	0.788	0.789	0.739	0.707
0.15	0.401	0.402	0.385	0.405
0.2	0.32	0.321	0.315	0.341
0.25	0.3	0.301	0.299	0.312
0.3	0.295	0.296	0.296	0.303
0.35	0.293	0.294	0.294	0.3
0.4	0.293	0.293	0.293	0.303
0.45	0.292	0.293	0.293	0.298
0.5	0.292	0.293	0.293	0.298
0.55	0.292	0.293	0.293	0.298
0.6	0.292	0.293	0.293	0.298

Table A3. IM electromagnetic torque T_e (pu).

t (s)	Model I	Model II	Model III	Model IV
0.01	2.461	2.460	2.491	2.392
0.05	1.424	1.424	1.459	1.34
0.1	-0.421	-0.421	-0.391	-0.481
0.15	-0.127	-0.127	-0.111	-0.161
0.2	-0.14	-0.14	-0.006	-0.031
0.25	0.027	0.027	0.03	0.019
0.3	0.041	0.042	0.043	0.038
0.35	0.047	0.047	0.048	0.045
0.4	0.049	0.049	0.049	0.048
0.45	0.049	0.05	0.05	0.049
0.5	0.05	0.05	0.05	0.05
0.55	0.05	0.05	0.05	0.05
0.6	0.05	0.05	0.05	0.05

References

1. Boldea, I. *Induction Machines Handbook: Transients, Control Principles, Design and Testing*; CRC Press: Boca Raton, FL, USA, 2020. [[CrossRef](#)]
2. Gregor, R. (Ed.) *Induction Motors: Applications, Control and Fault Diagnostics*; BoD—Books on Demand, InTech: Rijeka, Croatia, 2015.
3. Madhavan, S.; P B, R.D.; Gundabattini, E.; Mystkowski, A. Thermal Analysis and Heat Management Strategies for an Induction Motor, a Review. *Energies* **2022**, *15*, 8127. [[CrossRef](#)]
4. Khumalo, N.S.; Memane, N.P.; Akuru, U.B. Performance and Safety Improvement of Induction Motors Based on Testing and Evaluation Standards. *CES Trans. Electr. Mach. Syst.* **2024**, *8*, 310–318. [[CrossRef](#)]
5. Goman, V.; Prakht, V.; Kazakbaev, V.; Dmitrievskii, V. Comparative Study of Induction Motors of IE2, IE3 and IE4 Efficiency Classes in Pump Applications Taking into Account CO₂ Emission Intensity. *Appl. Sci.* **2020**, *10*, 8536. [[CrossRef](#)]
6. Orlova, S.; Konuhova, M.; Kamolins, E.; Otankis, R. Design of magnetic couplings for bioreactors: Analytical treatment and optimization. In Proceedings of the 2018 20th European Conference on Power Electronics and Applications (EPE'18 ECCE Europe), Riga, Latvia, 17–21 September 2018.
7. Suleiko, A.; Vanags, J.; Konuhova, M.; Dubencovs, K.; Grigs, O. The application of novel magnetically coupled mixer drives in bioreactors of up to 15 m³. *Biochem. Eng. J.* **2020**, *154*, 107464. [[CrossRef](#)]
8. Bezrukovs, V.; Bezrukovs, V.; Konuhova, M.; Bezrukovs, D.; Kaldre, I.; Popov, A.I. Numerical Simulations of Thermodynamic Processes in the Chamber of a Liquid Piston Compressor for Hydrogen Applications. *Technologies* **2024**, *12*, 266. [[CrossRef](#)]
9. Terlip, D. *Hydrogen Compressor Reliability Investigation and Improvement*; Cooperative Research and Development Final Report; CRADA Number CRD-13-514 (No. NREL/TP-5400-66027); National Renewable Energy Lab. (NREL): Golden, CO, USA, 2016. [[CrossRef](#)]
10. Bezrukovs, V.; Bezrukovs, V.; Konuhova, M.; Bezrukovs, D.; Berzins, A. Hydrogen hydraulic compression system for refuelling stations. *Latv. J. Phys. Tech. Sci.* **2022**, *59*, 96–105. [[CrossRef](#)]
11. J Chapman, S. *Electric Machinery Fundamentals*; McGraw-Hill: New York, NY, USA, 2004.
12. Agamloh, E.B.; Cavagnino, A. High efficiency design of induction machines for industrial applications. In Proceedings of the 2013 IEEE Workshop on Electrical Machines Design, Control and Diagnosis (WEMDCD), Paris, France, 11–12 March 2013; pp. 33–46. [[CrossRef](#)]
13. IEA Energy Efficient End-Use Equipment (4E). Available online: <https://www.iea-4e.org/emsa/> (accessed on 10 January 2025).
14. Okoro, O.I.; Ogbuka, C.U.; Agu, M.U. Simulation of dc machines transient behaviors: Teaching and research. *Pac. J. Sci. Technol.* **2008**, *9*, 142–148.
15. Beňová, M.; Dobrucký, B.; Šedo, J.; Praženica, M.; Koňarik, R.; Šimko, J.; Kuchař, M. A Novel Approach to Transient Fourier Analysis for Electrical Engineering Applications. *Appl. Sci.* **2024**, *14*, 9888. [[CrossRef](#)]
16. Navarro-Navarro, A.; Ruiz-Sarrío, J.E.; Biot-Monterde, V.; Antonino-Daviu, J.A.; Becker, V.; Urschel, S. Application of Transient Analysis Techniques to Fault Diagnosis in Low- and Medium-Power Synchronous Machines. *Machines* **2023**, *11*, 288. [[CrossRef](#)]
17. Mostajeran, E.; Amiri, N.; Ebrahimi, S.; Jatskevich, J. Electrical Machines in Electromagnetic Transient Simulations: Focusing on efficient and accurate models. *IEEE Electr. Mag.* **2023**, *11*, 38–53. [[CrossRef](#)]
18. Melkebeek, J.A. Transient Phenomena in Electrical Machines. In *Electrical Machines and Drives. Power Systems*; Springer: Cham, Switzerland, 2018. [[CrossRef](#)]
19. Zhu, J.H.; Zhang, P.; Tan, L.; Gu, J.; Li, H. Improved MSTOGI-PLL with enhanced control under non-ideal grid voltage conditions. *Electr. Power Syst. Res.* **2025**, *238*, 111060. [[CrossRef](#)]
20. Gnaciński, P.; Pepliński, M.; Muc, A.; Hallmann, D. Induction Motors Under Voltage Unbalance Combined with Voltage Subharmonics. *Energies* **2024**, *17*, 6324. [[CrossRef](#)]
21. Fachini, F.; de Castro, M.; Bogodorova, T.; Vanfretti, L. Modeling of Induction Motors and Variable Speed Drives for Multi-Domain System Simulations Using Modelica and the OpenIPSL Library. *Electronics* **2024**, *13*, 1614. [[CrossRef](#)]
22. Konuhova, M. Modeling of Induction Motor Direct Starting with and without Considering Current Displacement in Slot. *Appl. Sci.* **2024**, *14*, 9230. [[CrossRef](#)]
23. Cureño-Osornio, J.; Alvarez-Ugalde, C.A.; Zamudio-Ramirez, I.; Osornio-Rios, R.A.; Dunai, L.; Tsurcanu, D.; Antonino-Daviu, J.A. Start-Up and Steady-State Regimes Automatic Separation in Induction Motors by Means of Short-Time Statistics. *Electronics* **2024**, *13*, 3850. [[CrossRef](#)]
24. Kim, J.G. Soft Start Analysis of Induction Motor Using Current Phase Angle. *J. Electr. Eng. Technol.* **2022**, *17*, 1475–1480. [[CrossRef](#)]
25. Hannan, M.A.; Ali, J.A.; Ker, P.J.; Mohamed, A.; Lipu, M.S.H.; Hussain, A. Switching Techniques and Intelligent Controllers for Induction Motor Drive: Issues and Recommendations. *IEEE Access* **2018**, *6*, 47489–47510. [[CrossRef](#)]

26. Jidin, A.; Karim, K.A.; Rahim, K.; Raj, L.; Victor, L.; Ramahlingam, S.; Sutikno, T. A Review on Constant Switching Frequency Techniques for Direct Torque Control of Induction Motor. *Indones. J. Electr. Eng. Comput. Sci.* **2017**, *7*, 364–372. [[CrossRef](#)]
27. Farhadi, M.; Fard, M.T.; Abapour, M.; Hagh, M.T. DC–AC Converter-Fed Induction Motor Drive With Fault-Tolerant Capability Under Open- and Short-Circuit Switch Failures. *IEEE Trans. Power Electron.* **2018**, *33*, 1609–1621. [[CrossRef](#)]
28. Aree, P. Effects of unbalanced voltage on induction motor operating points under different load torque profiles. In Proceedings of the 2016 13th International Conference on Electrical Engineering/Electronics, Computer, Telecommunications and Information Technology (ECTI-CON), Chiang Mai, Thailand, 28 June–1 July 2016; pp. 1–4. [[CrossRef](#)]
29. Laadjal, K.; Sahraoui, M.; Alloui, A.; Cardoso, A.J.M. Three-Phase Induction Motors Online Protection against Unbalanced Supply Voltages. *Machines* **2021**, *9*, 203. [[CrossRef](#)]
30. Zhang, X.; Xu, G.; Chen, X.; Chen, R.; Chen, S.; Zhang, S. Three-Phase Unbalance Analysis Method Based on Three-Phase Motor Current Instantaneous Information. *Appl. Sci.* **2023**, *13*, 6127. [[CrossRef](#)]
31. Abdo, A.; Siam, J.; Abdou, A.; Shehadeh, H.; Mustafa, R. Practical Test on the Operation of the Three-Phase Induction Motor under Single-Phasing Fault. *Appl. Sci.* **2024**, *14*, 4690. [[CrossRef](#)]
32. Almounajjed, A.; Sahoo, A.K.; Kumar, M.K.; Bakro, M.W. Condition Monitoring and Fault Diagnosis of Induction Motor—An Experimental Analysis. In Proceedings of the 2021 7th International Conference on Electrical Energy Systems (ICEES), Chennai, India, 11–13 February 2021; pp. 433–438. [[CrossRef](#)]
33. Niu, G.; Dong, X.; Chen, Y. Motor Fault Diagnostics Based on Current Signatures: A Review. *IEEE Trans. Instrum. Meas.* **2023**, *72*, 3520919. [[CrossRef](#)]
34. Ganeriwala, S. Induction Motor Diagnostics Using Vibration and Motor Current Signature Analysis. In *Special Topics in Structural Dynamics & Experimental Techniques*; Allen, M., Blough, J., Mains, M., Eds.; Springer: Cham, Switzerland, 2024; Volume 5. [[CrossRef](#)]
35. Mirzaeva, G.; Saad, K.I.; Jahromi, M.G. Comprehensive Diagnostics of Induction Motor Faults Based on Measurement of Space and Time Dependencies of Air Gap Flux. *IEEE Trans. Ind. Appl.* **2017**, *53*, 2657–2666. [[CrossRef](#)]
36. Tang, J.; Yang, Y.; Blaabjerg, F.; Chen, J.; Diao, L.; Liu, Z. Parameter Identification of Inverter-Fed Induction Motors: A Review. *Energies* **2018**, *11*, 2194. [[CrossRef](#)]
37. Antonelli, S.L.; Donolo, P.D.; Pezzani, C.M.; Quispe, E.C.; De Angelo, C.H. Identification of induction motor parameters using genetic algorithms. In Proceedings of the 2023 IEEE Workshop on Power Electronics and Power Quality Applications (PEPQA), Cali, Colombia, 4–5 October 2023; pp. 1–7. [[CrossRef](#)]
38. Luo, X.; Zhao, J.; Xiong, Y.; Xu, H.; Chen, H.; Zhang, S. Parameter Identification of Five-Phase Squirrel Cage Induction Motor Based on Extended Kalman Filter. *Processes* **2022**, *10*, 1440. [[CrossRef](#)]
39. Véliz-Tejo, A.; Travieso-Torres, J.C.; Peters, A.A.; Mora, A.; Leiva-Silva, F. Normalized-Model Reference System for Parameter Estimation of Induction Motors. *Energies* **2022**, *15*, 4542. [[CrossRef](#)]
40. Udomsuk, S.; Areerak, K.; Areerak, T.; Areerak, K. Online Estimation of Three-Phase Induction Motor Parameters Using an Extended Kalman Filter for Energy Saving. *Energies* **2024**, *17*, 2115. [[CrossRef](#)]
41. Bednarz, S.A.; Dybkowski, M. Estimation of the Induction Motor Stator and Rotor Resistance Using Active and Reactive Power Based Model Reference Adaptive System Estimator. *Appl. Sci.* **2019**, *9*, 5145. [[CrossRef](#)]
42. Reddy, B.K.; Ayyagari, K.S.; Kumar, Y.P.; Giri, N.C.; Rajgopal, P.V.; Fotis, G.; Mladenov, V. Experimental Benchmarking of Existing Offline Parameter Estimation Methods for Induction Motor Vector Control. *Technologies* **2024**, *12*, 123. [[CrossRef](#)]
43. Klosowski, Z.; Fajfer, M.; Ludwikowski, Z. Reduction of the Electromagnetic Torque Oscillation during the Direct on Line (DOL) Starting of a 6 kV Motor by Means of a Controlled Vacuum Circuit-Breaker. *Energies* **2022**, *15*, 4246. [[CrossRef](#)]
44. *IEEE Std 3002.7-2018*; IEEE Recommended Practice for Conducting Motor-Starting Studies and Analysis of Industrial and Commercial Power Systems. IEEE: New York, NY, USA, 2019; pp. 1–107. [[CrossRef](#)]
45. Meshcheryakov, V.; Belousov, A. Development of a method for reducing starting currents and electromagnetic torque of a two-phase induction motor by delaying voltage supply. In Proceedings of the 2021 XVIII International Scientific Technical Conference Alternating Current Electric Drives (ACED), Ekaterinburg, Russia, 24–27 May 2021; pp. 1–5. [[CrossRef](#)]
46. Bonnett, A.H. The impact that voltage and frequency variations have on AC induction motor performance and life in accordance with NEMA MG-1 standards. In Proceedings of the Conference Record of 1999 Annual Pulp and Paper Industry Technical Conference (Cat. No. 99CH36338), Seattle, WA, USA, 21–25 June 1999; pp. 16–26. [[CrossRef](#)]
47. Chaban, A.; Łukasik, Z.; Popena, A.; Szafraniec, A. Mathematical Modelling of Transient Processes in an Asynchronous Drive with a Long Shaft Including Cardan Joints. *Energies* **2021**, *14*, 5692. [[CrossRef](#)]
48. Chen, X.; Gong, P. Transient and Steady-State Performance Improvement of IM Drives Based on Dual-Torque Model. *Machines* **2023**, *11*, 490. [[CrossRef](#)]

49. Basak, B. Transient behaviour of three phase induction motor under supply interruption of one phase during starting. In Proceedings of the National Power Systems Conference-IIT, Kharagpur, India, 27–29 December 2002; pp. 259–262.
50. Ahmed, A.; Ali, A.; Karrar, A.; Bowman, M.; Cooper, P. Estimating the Effects of Small Voltage and Frequency Changes on Industrial Induction Motor Loading. In Proceedings of the 2019 IEEE Power & Energy Society General Meeting (PESGM), Atlanta, GA, USA, 4–8 August 2019; pp. 1–5. [CrossRef]
51. Saucedo-Dorantes, J.J.; Jaen-Cuellar, A.Y.; Perez-Cruz, A.; Elvira-Ortiz, D.A. Detection of Inter-Turn Short Circuits in Induction Motors under the Start-Up Transient by Means of an Empirical Wavelet Transform and Self-Organizing Map. *Machines* **2023**, *11*, 958. [CrossRef]
52. Srndovic, M.; Fišer, R.; Grandi, G. Analysis of Equivalent Inductance of Three-Phase Induction Motors in the Switching Frequency Range. *Electronics* **2019**, *8*, 120. [CrossRef]
53. Yabaci, S.B.; Atalay, A.K.; AhmetKocabaş, D. Design of an innovative mathematical model for transient response of three phase induction machine. In Proceedings of the 2016 National Conference on Electrical, Electronics and Biomedical Engineering (ELECO), Bursa, Turkey, 1–3 December 2016; pp. 344–348.
54. Goolak, S.; Gubarevych, O.; Yermolenko, E.; Slobodyanyuk, M.; Gorobchenko, O. Mathematical modeling of an induction motor for vehicles. *East. Eur. J. Enterp. Technol.* **2020**, *2*, 104. [CrossRef]
55. Hamola, O.Y.; Maday, V.S.; Vasylychshyn, I.I. Mathematical Modelling of Starting Modes of Induction Motors with Squirrel-Cage Rotor. *Electr. Eng. Electromech.* **2021**, *2*, 9–15. [CrossRef]
56. Sengamalai, U.; Anbazhagan, G.; Thamizh Thentral, T.M.; Vishnuram, P.; Khurshaid, T.; Kamel, S. Three Phase Induction Motor Drive: A Systematic Review on Dynamic Modeling, Parameter Estimation, and Control Schemes. *Energies* **2022**, *15*, 8260. [CrossRef]
57. Le Roux, P.F.; Ngwenyama, M.K. Static and Dynamic Simulation of an Induction Motor Using Matlab/Simulink. *Energies* **2022**, *15*, 3564. [CrossRef]
58. Alitasb, G.K. Assessment of Fractional and Integer Order Models of Induction Motor Using MATLAB/Simulink. *Model. Simul. Eng.* **2024**, 2739649. [CrossRef]
59. Singh, M.; Chaturvedi, D.K. Simulink Model of Induction Motor Under Faulty Conditions. 12 May 2024. [CrossRef]
60. Dawood, A.; Ismeil, M.A.; Hussein, H.S.; Hasaneen, B.M.; Abdel-Aziz, A.M. An Efficient Protection Scheme Against Single-Phasing Fault for Three-Phase Induction Motor. *IEEE Access* **2024**, *12*, 6298–6317. [CrossRef]
61. Bahgat, B.H.; Elhay, E.A.; Elkholy, M.M. Advanced fault detection technique of three phase induction motor: Comprehensive review. *Discov. Electron.* **2024**, *1*. [CrossRef]
62. Boll, A.; Brokhausen, F.; Amorim, T.; Kehler, T.; Vogelsang, A. Characteristics, potentials, and limitations of open-source Simulink projects for empirical research. *Softw. Syst. Model* **2021**, *20*, 2111–2130. [CrossRef]
63. Blohm, P.; Herber, P.; Remke, A. Towards Quantitative Analysis of Simulink Models Using Stochastic Hybrid Automata. In *Integrated Formal Methods. IFM 2024*; Kosmatov, N., Kovács, L., Eds.; Lecture Notes in Computer Science; Springer: Cham, Switzerland, 2025; Volume 15234. [CrossRef]
64. LinkedIn. What Are the Advantages and Disadvantages of Using Simulink? Available online: <https://www.linkedin.com/advice/0/what-advantages-disadvantages-using-simulink> (accessed on 5 January 2025).
65. ResearchGate. Are You Familiar with Strengths and Weaknesses of Simulink to Simulate Power Systems? Available online: <https://www.researchgate.net/post/Are-you-familiar-with-strengths-and-weaknesses-of-Simulink-to-simulate-power-systems> (accessed on 5 January 2025).
66. Metcalf, M.; Reid, J.; Cohen, M. *Modern Fortran Explained: Incorporating Fortran 2018*; Oxford University Press: Oxford, UK, 2018.
67. Kopylov, I.P. *Mathematical Models of Electric Machines*; Mir Publishers: Moscow, Russia, 2001; p. 155.
68. Dirba, J.; Ketners, K. *Elektriskās mašīnas [Electrical Machines]*; RTU Publishing House: Riga, Latvia, 2009.
69. Muchande, S.; Kadam, A.; Unni, K.; Thale, S. Design and Implementation of a Direct Torque Control Space Vector Modulated Three Phase Induction Motor Drive. In *Advances in Computing, Communication, and Control. ICAC3 2013*; Unnikrishnan, S., Surve, S., Bhoir, D., Eds.; Communications in Computer and Information Science; Springer: Berlin/Heidelberg, Germany, 2013; Volume 361. [CrossRef]
70. Qu, R.; Zhou, Y.; Milestones, D.L. Hotspots and trends in the development of electric machines. *iEnergy* **2022**, *1*, 82–99. [CrossRef]
71. Fu, W.N.; Liu, Y. A unified theory of flux-modulated electric machines. In Proceedings of the 2016 International Symposium on Electrical Engineering (ISEE), Hong Kong, China, 14 December 2016; pp. 1–13. [CrossRef]
72. Bramerdorfer, G.; Tapia, J.A.; Pyrhönen, J.J.; Cavagnino, A. Modern Electrical Machine Design Optimization: Techniques, Trends, and Best Practices. *IEEE Trans. Ind. Electron.* **2018**, *65*, 7672–7684. [CrossRef]
73. Ključev, V.I. *Theory of Electric Drives: Textbook for Universities*; Energoizdat: Moscow, Russia, 1985.
74. Slemmon, G.R. Modelling of induction machines for electric drives. *IEEE Trans. Ind. Appl.* **1989**, *25*, 1126–1131. [CrossRef]
75. Gao, J.D.; Zhang, L.Z.; Wang, X.H. *AC Machine Systems*; Tsinghua University Press: Beijing, China, 2009. [CrossRef]

76. Sobolevskaya, A.E.; Shlaf, M.M.; Afonin, V.I.; Sobolevskaya, E.A. *Asynchronous Motors of the 4A Series: Handbook*; Energoizdat: Moscow, Russia, 1982.
77. Han, D.; Qi, H.; Wang, S.; Hou, D.; Wang, C. Adaptive Step-size Forward–Backward Pursuit and Acoustic Emission-Based Health State Assessment of High-Speed Train Bearings. *Structural Health Monitoring*. 2024. Available online: <http://sage.cnperreading.com/paragraph/article/?doi=10.1177/14759217241271036> (accessed on 28 January 2025).

Disclaimer/Publisher’s Note: The statements, opinions and data contained in all publications are solely those of the individual author(s) and contributor(s) and not of MDPI and/or the editor(s). MDPI and/or the editor(s) disclaim responsibility for any injury to people or property resulting from any ideas, methods, instructions or products referred to in the content.